Adsorption of the Neutral Macromonomeric Surfactant Tween-80 at the Mercury/Electrolyte Solution Interface as a Function of Electrode Potential and Time

ARTICLE *in* LANGMUIR · JUNE 2000

Impact Factor: 4.46 · DOI: 10.1021/la991434e

Adsorption of the Neutral Macromonomeric Surfactant Tween-80 at the Mercury/Electrolyte Solution Interface as a Function of Electrode Potential and Time

A. Avranas,* N. Papadopoulos, D. Papoutsi, and S. Sotiropoulos

Laboratory of Physical Chemistry, Department of Chemistry, Aristotle University, 54006 Thessaloniki, Greece

Received November 1, 1999. In Final Form: April 7, 2000

The adsorption of the neutral macromonomeric surfactant Tween-80 from electrolyte solutions on a polarized mercury electrode was studied by means of differential capacitance measurements of the electrode double layer. Its variation with potential and time can provide qualitative information on the state of the Tween-80 adsorbate. The time evolution of the phenomenon is followed by sampling the capacitive current at different time periods after stepping the electrode potential at given values, and the steady-state differential capacitance (C) vs electrode potential (E) curve is obtained from long-duration data. Features associated with surface aggregation processes, such as capacitance plateaus, deformed peaks, and increase in capacitance with increasing time or surfactant concentration, start to appear even at concentrations below the bulk critical micelle concentration (cmc). The type of surface aggregates (surface micelles) formed depends on surface coverage and orientation which vary with time and surfactant bulk activity up to the cmc value. This continuous change of the surface state with bulk concentration gives rise to a rather continuous change of the corresponding C vs E characteristics. Two distinct capacitance plateaus are observed for the higher concentrations studied and are attributed to two-dimensional surface micelles of different monomer-unit orientations, but (unlike the charged micelles studied previously) these surface micelles do not collapse at extreme potentials into condensed polylayers. The very slow attainment of a steady state even at high concentrations is indicative of a surfactant surface concentration and orientation (and, hence, state too) which are dependent on the slow three-dimensional interaction of the first adsorption layer with outer adsorbed layers.

Introduction

Nonionic surfactants used as solubilizers of organics in aqueous solutions, emulsion stabilizers, and extraction agents in ternary water−oil−organic solute systems are important for a variety of applications in the pharmaceutical, cosmetic, food, and agrochemical industries.[1−6] Tween-80 (polyoxyethylene(20) sorbitan mono-oleate) (Figure 1a), a common neutral amphiphile, forms, at concentrations above its cmc, typical macromonomeric (known also as polymeric) aggregates—micelles which differ from the spherical micelles of ionic surfactants in that the macromonomeric micelles grow into rodlike objects.[7] The size, shape, and self-diffusion coefficients of Tween-80 primary and secondary micelles above the first and second cmc values have been studied by a variety of cyclic voltammetric and spectroscopic (NMR, fluorescence) techniques[7−9] and are found to be critically dependent on the hydration of their hydrophilic parts. At higher bulk concentrations, Tween-80 forms liquid crystals.[10,11]

The adsorption of Tween-80 at interfaces other than the air/aqueous solution and the organic/aqueous phase, particularly at solid surfaces, is important in species extraction from or onto a solid substrate,[2,12] modification of membranes by adsorbed surfactants,[13] and penetration of micelle-encapsulated drugs into the skin.[6]

The adsorption of Tween-80 at the mercury electrode/electrolyte solution interface (a model charged interface) has been previously studied by means of differential capacitance measurements by Müller and Dörfler[14] and by Sotiropoulos et al.[15] and Antoniou et al.[16] as a part of an extensive theoretical[17−19] and experimental[15,16,20−25]

* Corresponding author. Tel: 0030−31−997686. Fax: 0030−31−997709. E-mail: avranas@chem.auth.gr.

(1) Ko, S. O.; Schlautman, M. A.; Carraway, E. R. *Environ. Sci. Technol.* **1998**, *32* (18), 2769.
(2) Taha, M. R.; Soewarto, I. H.; Acar, Y. B.; Gale, R. J.; Zappi, M. E. *Water, Air, Soil Pollut.* **1997**, *100* (1−2), 33.
(3) Friberg, S. E.; Huang, T.; Aikens, P. A. *Colloids Surf., A* **1993**, *121* (1), 1.
(4) Akay, G.; Brown, I. J.; Sotiropoulos, S.; Lester, E. *Mater. Lett.* **1998**, *35*, 383.
(5) Salmeron, M. D.; Hernandez, P. J.; Cerezo, A. *Drug Dev. Ind. Pharm.* **1997**, *23* (2), 133.
(6) Arellano, A.; Sandoyo, S.; Martn, C.; Ygartua, P. *Eur. J. Drug Metab. Pharmacokinet.* **1998**, *23* (2), 307.
(7) Geetha, B.; Mandal, A. B. *J. Chem. Phys.* **1996**, *105* (21), 9649.
(8) Geetha, B.; Mandal, A. B. In *IUPAC Sponsored International Symposium on Surface and Colloid Science and Its Relevance to Soil Pollution and 6th National Conference on Surfactant, Emulsions and Biocolloids*; Madras, India, 1994; p 317.
(9) Geetha, B.; Mandal, A. B. *Langmuir* **1995**, *11*, 1464.
(10) Tiddy, G. J. T.; Walsh, M. F. *Stud. Phys. Theor. Chem.* **1983**, *26*, 151.
(11) Rong, G.; Yang, J.; Friberg, S. E. *Langmuir* **1996**, *12* (17), 4286.
(12) Santhanalakshmi, J.; Balaji, S. *J. Colloid Interface Sci.* **1996**, *179*, 517.
(13) Redy, S. M.; Vadgama, P. M. *Anal. Chim. Acta* **1997**, *350* (1−2), 77.
(14) Müller, E.; Dörfler, H.-D. *Tenside Deterg.* **1977**, *14*, 75.
(15) Sotiropoulos, S.; Nikitas, P.; Papadopoulos, N. *J. Electroanal. Chem.* **1993**, *356*, 225.
(16) Antoniou, S.; Nikitas, P. *Electrochim. Acta* **1996**, *41* (16), 2613.
(17) Nikitas, P. *J. Electroanal. Chem.* **1991**, *300*, 607.
(18) Nikitas, P.; Sotiropoulos, S.; Papadopoulos, N. *J. Phys. Chem.* **1992**, *96*, 84522.
(19) Nikitas, P; *J. Electroanal. Chem.* **1993**, *348*, 59.
(20) Sotiropoulos, S.; Nikitas, P.; Papadopoulos, N. *J. Electroanal. Chem.* **1993**, *356*, 201.
(21) Papadopoulos, N.; Sotiropoulos, S.; Nikitas, P. *J. Electroanal. Chem.* **1992**, *324*, 375.
(22) Papadopoulos, N.; Sotiropoulos, S.; Nikitas, P. *J. Colloid Interface Sci.* **1992**, *151*, 523.
(23) Papadopoulos, N.; Avranas, A.; Sotiropoulos, S. *Bioelectrochem. Bioenergetics* **1992**, *29*, 223.
(24) Avranas, A.; Papadopoulos, N.; Sotiropoulos, S. *Colloid Polym. Sci.* **1994**, *272*, 1252.

10.1021/la991434e CCC: $19.00
Published on Web 06/17/2000

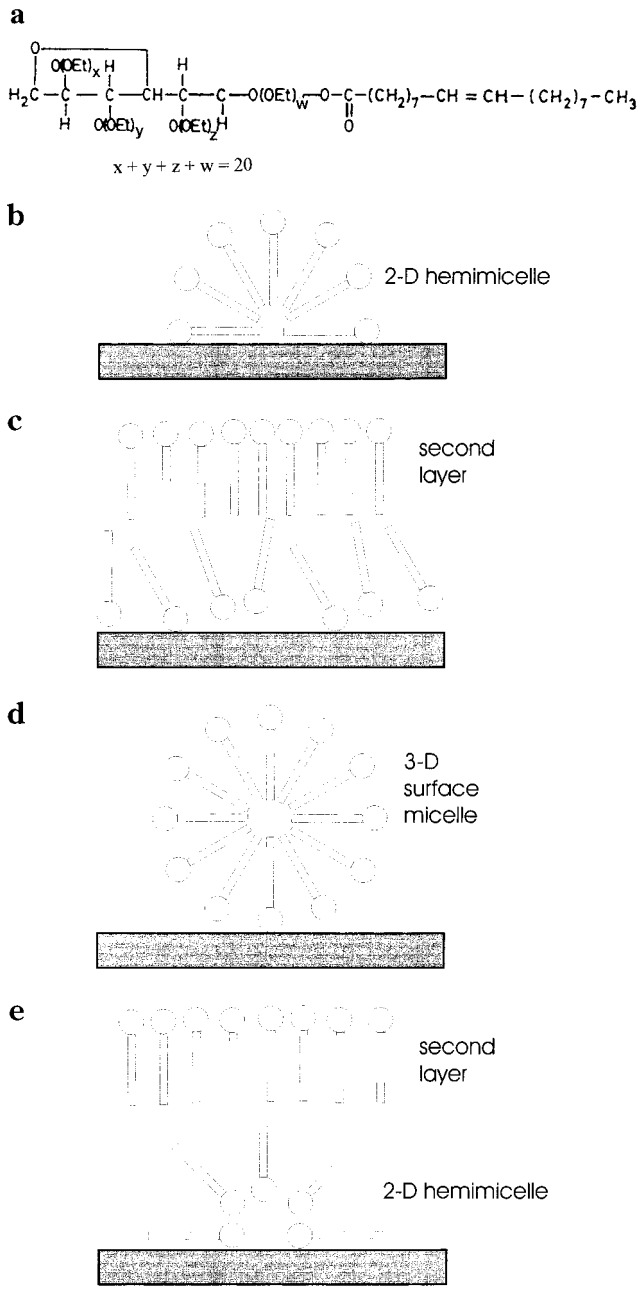

Figure 1. The molecular structure of the Tween-80 monomer (a) and various possible arrangements of its surface aggregates on a polarized electrode surface: (b) $E > E_{pzc}$, (c), (d) $E \approx E_{pzc}$, (e) $E < E_{pzc}$.

study of surfactant adsorption at the Hg electrode. The adsorption of organics at the polarized Hg electrode results in the replacement of water molecules and specifically adsorbed ions from the electrode double layer, hence causing significant changes in the corresponding capacitor.[26] The differential capacitance (C) of the double layer formed between the charged electrode and a surfactant electrolyte solution can be easily measured by ac perturbation techniques as a function of electrode potential (E) and/or time (t), resulting in characteristic C vs E and C vs t curves. In many cases, due to strong adsorbate−adsorbate or substrate−adsorbate interactions, the adsorbed species undergo phase changes as the adsorbate concentration and/or the electrode potential are varied; at the molecular level, the phase changes can be interpreted as reorientation, formation of surface salts or aggregates, compact film formation, etc.[27]

On the basis of application of the Avrami theorem[28] for two-dimensional phase formation and the power law of nucleation derived in ref 29 to metal electrodeposition[30] and adsorption,[31] the kinetics of compact film formation at the electrode surface have often been analyzed in terms of nucleation and growth rates.[29−33]

According to a recent thermodynamic classification of phase transitions at charged interfaces,[17] there are two general types of phase changes of an adsorbed layer that can take place on electrodes: surface-phase separation, where at least one of the coexisting phases at equilibrium corresponds to a saturated surface solution of the adsorbate in coadsorbed solvent, and two-dimensional condensation, occurring between states of the interface corresponding to an adsorbate surface coverage equal to unity. Surface micellization, i.e., the formation of surface aggregates, is a special case of the first type of transition. Among the criteria for a surface phase transition to occur reversibly is constant electrode potential (E) as the electrode charge density (σ^M) changes in a stepwise fashion during the transition.[17] This results in an abrupt, needlelike change of the differential capacitance with electrode potential, since $C = d\sigma^M/dE$. However, in the special case of surface micellization, where one of the surface states is a micellar phase, some deviation from the above picture should be expected. That is, we must take into consideration that micelles are usually regarded as a microphase rather than a typical, macroscopic phase. Then according to the theory of thermodynamics of small systems[34] developed by Hill, a phase change leading to the formation/deformation of small micelles is realized in a less abrupt manner than in the phase change leading to large micelles. That is, the plot of a specific variable, such as the electrode charge density, versus an intensive one, such as the electrode potential, does not show a vertical step but an inflection point when surface micelles are formed/deformed. Then a bell-shaped capacitance maximum should be expected for a phase transition between surface micelles and a saturated surface solution of adsorbate monomers. The height and shape of these peaks depends almost exclusively on the number of monomer units of the surface aggregates[19] and not in a straightforward manner on concentration (although simple adsorption/desorption peaks do[26]). As the number of monomer units increases, the peaks become higher, sharper, and more asymmetric, with one abrupt vertical side.[19] From the thermodynamic point of view, surface aggregates with a number of monomer units $N \rightarrow \infty$ are indistinguishable from a compact layer macrophase, since the transformation of both into a new phase will lead to a needlelike capacitance peak.[35]

As the bulk adsorbate and the interfacial adsorbate concentrations are increased, multilayer adsorption within

(25) Sotiropoulos, S.; Avranas, A.; Papadopoulos, N. *Langmuir* **1996**, *41* (16), 2613.
(26) Damaskin, B. B.; Petrii, O. A.; Batrakov, V. V. In *Adsorption of Organic Compounds at Electrodes*; Plenum Press: New York, 1971.
(27) Buess-Herman, C. In *Trends in Interfacial Electrochemistry*; Silva, A. F., Ed.; Plenum Press: New York, 1986.
(28) Avrami, M. *J. Chem. Phys.* **1939**, *7*, 1103; **1940**, *8*, 212.
(29) Jacobs, P. W. M.; Tompkins, F. C. In *The Chemistry of the Solid State*; Gardner, W., Ed.; Butterworth: London, 1955; Chapter 7.
(30) Fleischmann, M.; Thirsk, H. R. *Adv. Electrochem. Eng.* **1963**, *3*, 123.
(31) Retter, U. *J. Electroanal. Chem.* **1978**, *87*, 181.
(32) Retter, U. *J. Electroanal. Chem.* **1984**, *179*, 25.
(33) Budevski, E.; Staikov, G.; Lorenz, W. J. In *Electrochemical Phase Formation and Growth*; VCH: New York, 1996; Chapter 8.
(34) Hill, T. L. *Thermodynamics of Small Systems*; Benjamin: New York, 1963−1964; Vols. 1 and 2.
(35) De Levie, R.; *Chem. Rev.* **1988**, *88*, 599.

a multilayer interface can occur. Each sublayer of the interface could have its own transition electrode potential, i.e., its own potential value for which a monomer surface solution−surface micellar phase transition can occur; if these values differed significantly from sublayer to sublayer, then marked deformation or an even split of the corresponding phase transition capacitance peaks would be expected. The same situation could also arise if the transformation of the first monolayer were realized in successive phase transitions involving its interaction with outer layers and the formation of surface aggregates. Finally, such distorted peaks could be due to the partial convolution of two processes: one corresponding to the phase change and one to the adsorption/desorption of the surfactant. These pronounced capacitance peak deformations were observed for all the surfactants we studied.[16,20−25] Direct spectroscopic evidence of multilayer adsorption and phase changes via interfacial aggregates that extend in three dimensions has been recently reported for stearic acid adsorption on a gold single-crystal electrode.[36]

In the most recent paper[25] in the series of our relevant publications, we have established (apart from the abovementioned thermodynamic criteria applied to steady-state *C* vs *E* curves) a few empirical criteria for the formation of two- and three-dimensional surface micelles, based on *C* vs *t* transients recorded for the anionic and cationic surfactants we studied.[20−25] First of all, the Avrami plots corresponding to potential regions where surface aggregation/micellization is expected are only linear over limited time periods, and even then, they have noninteger slopes. Secondly, in regions where three-dimensional interactions between adsorbate units of different layers are expected (accompanied by reorientation or formation of three-dimensional surface micelles), capacitance transients that show a minimum are recorded. It should be noted that most of these surface transformations were found to be closely dependent on time over periods of a few minutes and that continuous sampling of the capacitive current was performed at fixed intervals to follow the evolution of the phenomenon in time (see Experimental Procedures).

Certain models have been proposed in the past to account for similar peculiarities in the *C* transients of some film formations.[37,38] The different values of steady-state minimum capacities recorded at different electrode potentials for 2-thiohydantoin were attributed less to film coverage than to unity with the rate of desorption from and adsorption onto condensed islands at dynamic equilibrium.[37] A rise in the *C* vs *t* curves for octanoic acid was theoretically described by the adsorption-controlled replacement of one condensed state by another.[38]

The aim of the present work is to further investigate the nature of the various Tween-80 surface aggregates that were speculated to form at the Hg/electrolyte solution interface from near-steady *C* vs *E* curves,[16] this time based on *C* vs *t* transients and long time, steady-state *C* vs *E* curves. The bulk cmc value and micelle aggregation number in solution were estimated from fluorescence and time-resolved fluorescence probing.[39] A comparison of the adsorption behavior of this neutral and bulky macromonomeric surfactant with that of the ionic monomeric surfactants previously studied is also made.

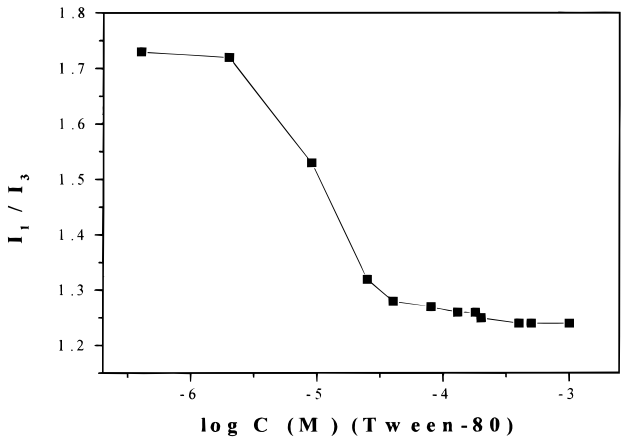

Figure 2. Values of the intensity ratio I_1/I_3 of the first and third vibronic peaks in the fluorescence emission spectrum of pyrene, plotted against surfactant concentration.

Experimental Procedures

Materials. Tween-80 was puriss quality (Ph. Eur. for bacteriology) obtained from Fluka and used as received. Na_2SO_4 from Fluka (puriss p.a. 99.5%) served as the supporting electrolyte. No minimum was observed in the surface tension versus the logarithm of concentration curves of the aqueous solutions of Tween-80 and Na_2SO_4, indicating the absence of surface-active impurities. Pyrene, used in fluorescence-probing experiments, was purchased from Fluka (puriss) and was used without further purification. High-purity Millipore water used in all sample preparations, and measurements were performed at 20 °C.

Surface Tension Measurements. The surface tensions of Tween-80 and Na_2SO_4 solutions were measured with a Krüss electronic tensiometer K10, employing the Wilhelmy plate method.[40] The accuracy of the measurements was estimated to be within ±0.2 mN/m. The cmc for Tween-80 in 0.1 M Na_2SO_4 aqueous solution was ca. 2.5×10^{-5} M at 20 °C.

Fluorescence-Probing Experiments. Fluorescence probing was used to determine the cmc of Tween-80 in aqueous solutions of sodium sulfate. For that, we used the value of the intensity ratio I_1/I_3 of the first and third vibronic peaks in the fluorescence emission spectrum of pyrene.[41] A home-assembled luminescence spectrometer was used for these measurements.

The aggregation number of Tween-80 bulk micelles was determined using the time-resolved fluorescence-quenching technique.[39] Time-resolved luminescence measurements were made by a photon-counting technique using a specially constructed hydrogen flash, as well as ORTEC and Schlumbeerger-Electric electronic instruments. The decay profiles were analyzed via least-squares fits using the distribution and the autocorrelation function of the residuals as fitting criteria. All samples were deoxygenated via bubbling with nitrogen.

When the Tween-80 concentration is below its cmc, the pyrene fluorescence spectrum exhibits its characteristics in a polar medium. As the micelles are formed, pyrene—which is a hydrophobic molecule–is dissolved in the micelles, close to the hydrophobic part of surfactant molecules, and the emission spectrum of pyrene in a nonpolar solvent is observed. The I_1/I_3 ratio in the emission spectrum of pyrene indicates the polarity sensed by pyrene at its solubilization site. Figure 2 shows the variation of the intensity ratio I_1/I_3, of the first and third vibronic peaks with surfactant concentration in the fluorescence emission spectrum of pyrene. The decrease in I_1/I_3 values indicates that the surfactant monomers aggregate and form micelles when the surfactant concentration is higher than about 2×10^{-5} M. To

(36) Bizzotto, D.; Lipkowski, J. *J. Electroanal. Chem*. **1996**, *409*, 33.
(37) Schrettenbrunner, M.; Chaiyasith, H.; Baumgärtel, H.; Retter, U. *Ber. Bunsen-Ges. Phys. Chem*. **1993**, *97*, 847.
(38) Retter, U.; Avranas, A.; Lohse, H.; Siegler, K.; Lunkenheimer, K. *Langmuir* **1999**, *15*, 3661.
(39) Zana, R. In *Surfactant Solutions. New Methods of Investigation*; Zana, R., Ed.; Marcel Dekker: New York, 1987, Chapter 5, p 241.
(40) Gaines, G. L. In *Insoluble Monolayers at Liquid−Liquid Interfaces*; Wiley: New York, 1966; p 44.
(41) Kalyanasundaran, K.; Thomas, J. K. *J. Am. Chem. Soc.* **1977**, *99*, 2039.

Table 1. Values of the Surfactant Aggregation Number *N* at Different Surfactant Concentrations, with and without Salt Addition

	N	
[Tween 80], *M*	without Na_2SO_4	with 0.1 M Na_2SO_4
10^{-4}	21	40
10^{-3}	96	133

determine the aggregation number in the bulk solution, we solubilized pyrene as a fluorescence probe and monitored the time-resolved fluorescence quenching due to excimer formation. The monomer pyrene fluorescence decay profiles were analyzed using a well-known model often used to study a variety of problems associated with micellar structure and dynamics.[42,43]

Table 1 shows the values of the micelle aggregation number *N* for two different surfactant concentrations, both in the presence and in the absence of salt/electrolyte. The increase of *N* with increasing surfactant concentration has also been reported.[44] As expected, the size of micellar aggregates increases with the addition of electrolyte at a given surfactant concentration, and Tween-80, as a typical neutral surfactant, forms relatively large micelles in solution.

Electrochemical Method and Instrumentation. The capacitive current of the double layer formed between a hanging mercury drop electrode (HMDE) and aqueous 0.1 M Na_2SO_4 solutions of Tween-80 was recorded by means of ac phase-sensitive chronoamperometry, following the application of the potential of interest, using a PAR model 170 electrochemistry system interfaced to an AT compatible PC (VIP 200, 12 MHz) via a 14 bit AD/DA card. The ac modulation was 5 mV p−p at 370 Hz, and the in-phase (0°) and out-of-phase (90°) components of the alternating current were recorded. At 370 Hz, the out-of-phase component could be taken as the capacitive current with a 1−2% accuracy. The transformation of this capacitive current to differential capacitance values was done by calibration based on the standard data provided by Grahame for KCl solutions.[45] Each mercury drop was formed within a 3 s period at −1.9 V vs a saturated calomel electrode (SCE, reference electrode to which all potentials in this paper are referred), where preliminary dropping mercury electrode (DME) experiments for short drop times showed no Tween-80 adsorption[15] (this can also be deduced by comparison of the similar values of the surfactant *C* vs *E* curves with that of the Na_2SO_4 base solution near −1.9 V, shown below in Results and Discussion). To produce drops of standard size, we adjusted an isochronous motor (5 rpm rotation speed) on top of the vernier whose turning controlled the size of the mercury drop at the end of the capillary of the Metrohm type E410 HMDE apparatus. The rotation of the motor producing drops of reproducible size was controlled by the computer via a relay. The electrode surface was calibrated using Grahame's data for the differential capacitance of a mercury electrode in contact with a solution containing 1 M KCl, the supporting electrolyte.[45] Preliminary experiments proved that with this experimental setup, the drop's size reproducibility was accurate to within 1%. To achieve even better accuracy in our results, we measured the capacitive current at the birth potential (−1.9 V) just before the application of the potential step. This value was stored in a file on the computer disk and was used to correct for the actual drop surface. At the end of each experiment pulse, the mercury drop was dislodged by intense deaeration, which was controlled by an electromagnetic relay. The experiments were performed successively in 10 mV intervals for the entire potential range *E* studied (i.e., from −1.8 to 0 V), and the capacitive current was sampled every 0.25 s. The entire *C* vs *E* curve was afterward constructed for selected time values ranging from fractions of a second to more than 60 s. More details about the sampled-current phase-sensitive ac voltammetric technique can be found in our series of publications.[21−25]

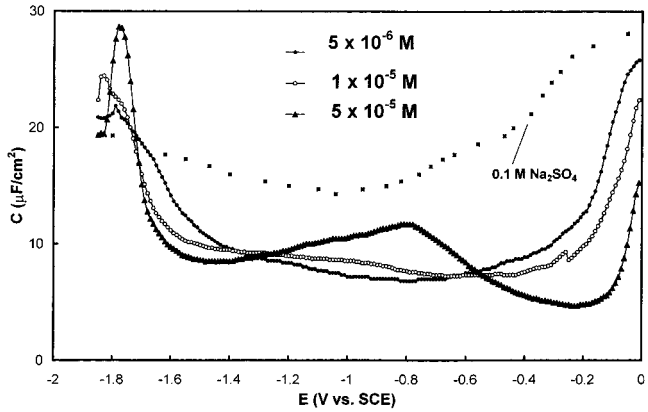

Figure 3. Differential capacitance (*C*) vs electrode potential (*E*) curves, constructed from data sampled at 90 s, for the interface between an HMDE and 0.1 M Na_2SO_4 aqueous solutions of 5×10^{-6}, 1×10^{-5}, and 5×10^{-5} M Tween-80, as well as the base solution of 0.1 M Na_2SO_4.

Results and Discussion

The steady-state differential capacitance (*C*) vs applied electrode potential (*E*) curves (corresponding to data collected for 90 s, long after the capacitive current had stopped changing) recorded for a HMDE in aqueous solutions of Tween-80-containing 0.1 M Na_2SO_4 are presented in Figure 3 for two pre-micellar (5×10^{-6} and 1×10^{-5} M) and one postmicellar (5×10^{-5} M) Tween-80 concentration. The general features of the curves, i.e., the extended plateaus of low capacitance, the extended hump that separates them (higher concentrations), and the deformed peak at negative potentials (lower concentrations), are in good agreement with the results presented in Figures 7 and 8 of ref 15, which corresponded to a near-steady-state, slow-potential sweep experiment at 2 mV/s. However, the *C* vs *E* curves of the present work, obtained under constant potential chronoamperometric conditions, vary more clearly with concentration, and both the negative peak and the capacitance hump are much better defined. It should be noted again that although these curves resemble typical phase-sensitive AC voltammograms, they are constructed from isochronous capacitance data sampled during many AC phase-sensitive chronoamperometric experiments.

A general feature of the *C* vs *E* curves over the entire potential range is their marked variation with time, which, depending on the concentration and potential range, can be up to 90 s, as shown in Figure 4 (main graph) for 5×10^{-5} M Tween-80. The variation of the *C* vs *E* curves with time is even more pronounced at extreme polarization, where the shape, height, and position of the capacitance peaks are seen to be critically dependent on time. This suggests that, if the characteristics of these peaks are to be correlated to the Tween-80 bulk cmc according to the empirical criteria developed by Vollhardt[46] or interpreted according to the theory of phase transitions involving surface aggregates developed by Nikitas et al.,[17,18] only the long-duration curves can safely be considered as near-equilibrium ones. Such long-duration variations as those depicted in Figure 4 (encountered even at the higher concentrations), exceed those expected for a simple diffusion process and imply that the phenomenon is governed by either slow adsorption kinetics or slow-proceeding phase transformations. This is also supported by the shape of *C* vs $t^{1/2}$ plots, given in Figure 5, for both the pre-micellar 1×10^{-5} (main graph) and the post-

(42) Lang, J.; Jada, A.; Malliaris, A. *J. Phys. Chem.* **1988**, *92*, 1946.
(43) Almgren, M. *Adv. Colloid Interface Sci.* **1992**, *41*, 9.
(44) Acharya, K.; Bhattacharya, S, C.; Moulik, S. P. *J. Photochem. Photobiol., A* **1997**, *109*, 29.
(45) Grahame, D. *J. Am. Chem. Soc.* **1949**, *71*, 2975.
(46) Vollhardt, D.; *Colloid Polym. Sci.* **1969**, *229*, 15; **1976**, *254*, 64.

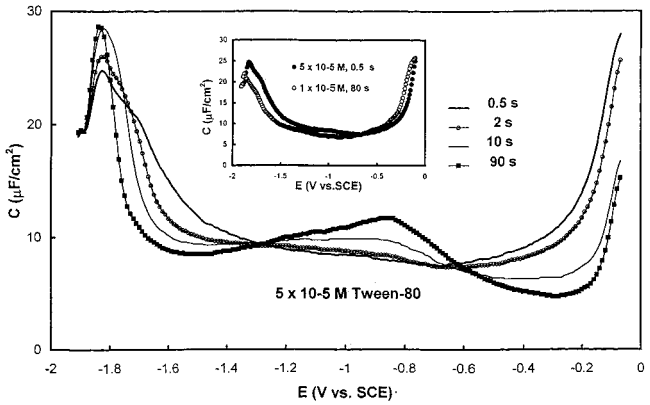

Figure 4. Differential capacitance (*C*) vs electrode potential (*E*) curves, constructed from data sampled at selected times for the interface between an HMDE and a 0.1 M Na_2SO_4 aqueous solution of 5×10^{-5} M Tween-80. Inset: Differential capacitance (*C*) vs electrode potential (*E*) curves for 5×10^{-5} M Tween-80 at 0.5 s and for 1×10^{-5} M Tween-80 at 80 s.

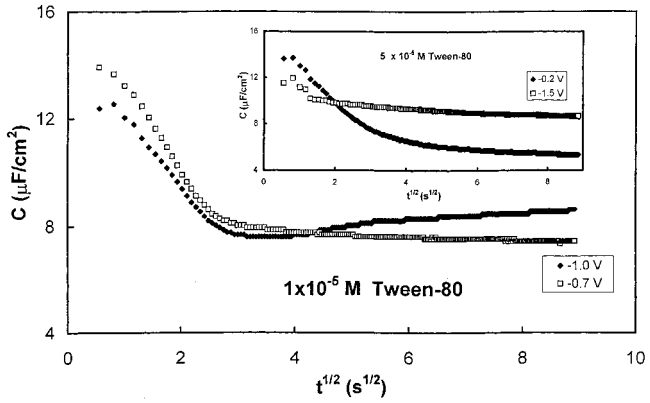

Figure 5. *C* vs $t^{1/2}$ curves for 1×10^{-5} M Tween-80 (at −1.0 and −0.7 V) and (Inset) for 5×10^{-5} M Tween-80 (at −0.2 and −1.5 V).

micellar 5×10^{-5} M (inset graph) concentrations. A simple diffusion-controlled adsorption process is described by the Koryta equation:[47]

$$\Gamma = 2c_b(Dt/\pi)^{1/2} \quad (1)$$

where Γ is the surface concentration of the adsorbate and c_b and *D* are its bulk concentration and diffusion coefficient, respectively. The adsorbate surface coverage is given[26] by

$$\theta = \Gamma/\Gamma_{max} \quad (2)$$

where Γ_{max} is the maximum-saturation surface concentration of the adsorbate determined by its molecular surface area. Taking into account the $\theta-C$ relationship given by eq 1 above, it follows that a *C* vs $t^{1/2}$ curve should be linear for a diffusion-controlled adsorption process. However, neither of the curves in Figure 5 is linear over any appreciable range, indicating that even for lower concentrations, diffusion is not the sole rate-controlling step.

From the inset of Figure 4, which shows that the short-duration (0.5 s) curve for the high concentration (5×10^{-5} M) is very similar to the long-duration (80 s) curve for the low concentration (1×10^{-5} M), it follows that the initial adsorbate states from postmicellar Tween-80 solutions are the same as those from pre-micellar solutions. This is an indication that the same entity is initially adsorbed on the electrode surface, i.e., the Tween-80 monomers in both cases, and that the adsorbate's phase changes are initially the same (formation of two-dimensional aggregates, as discussed later on). At high concentrations though, the adsorbate state continues to change with time, indicating a slow adsorption and/or interaction process of additional adsorbate with the first adsorption layer.

The presentation and discussion of results that follows is split into three parts. In the first part, we discuss the features of steady-state (90 s) *C* vs *E* curves, we attempt to classify the phase changes occurring at the interface as the electrode potential or concentration changes, and we comment on the possible adsorbate state at the molecular level. In the second part, we present some of the theoretical models describing film formation that appear in the literature. Finally, in the third part, *C* vs *t* transients after potential steps at characteristic polarization regions are given and the kinetics of the formation of the various adsorbate states are investigated.

Steady-State *C* vs *E* Curves. At all concentrations above 5×10^{-5} M (Figure 3), the *C* vs *E* curves coincide; i.e., no significant change is observed beyond the cmc point. Below this point, however, there is a continuous change of the picture with changing concentration. As the concentration increases, the deformation of the cathodic peak gradually disappears, but two distinct capacitance plateaus are formed.

The complex *C* vs *E* curve for all the concentrations (deformed cathodic peaks whose heights do not vary with concentration in a logarithmic manner, who have more than one minima, etc.), together with the pronounced hysteresis upon the potential sweep reversal presented in ref 16, indicates that the adsorption of Tween-80 on the mercury electrode is accompanied by aggregation phenomena. The fact that the minimum of the capacitance curves, which corresponds to the thicker and denser arrangement of the adsorbed layer, varies with bulk surfactant concentration up to the cmc point can be explained by dependence of the adsorbate state on surface concentration. The latter increases with increasing surfactant bulk concentration, while the adsorbed water concentration decreases at the same time; these concentration changes are likely to affect the size of surface aggregates in the same way that they affect the size of bulk aggregates (see the spectroscopic results in Experimental Procedures): an increase in surfactant concentration gives rise to larger micelles. Beyond the cmc value, the activity of the surfactant in the bulk solution remains constant and, hence, so do the adsorbate surface concentration and the corresponding surface aggregate state.

For the two pre-micellar concentrations in Figure 3, there is a moderately low capacitance region from ca. −0.3 to −1.5 V that is quite different both from the capacitance pits normally attributed to a condensed adsorbate film, often referred to as a "compact layer",[27,35] and from the capacitance plateaus of simple adsorption processes.[26] First of all, the corresponding state of the interface is terminated at negative and positive polarizations not by sharp, abrupt steps[27,35] but by curved capacitance branches that, at negative polarization, take the form of broad, deformed capacitance peaks. Secondly, there is no straightforward decrease of the capacitance value with increasing surfactant bulk concentration, as in the case of simple adsorption;[26] in fact, there is a potential region (ca. −0.7 to −1.4 V) where the capacitance increases with increasing concentration. This corresponds to a change in the adsorbate state, probably due to a change in its interfacial concentration and orientation, which results from a change

(47) Koryta, J. *Collect. Czech. Chem. Commun.* **1953**, *18*, 206.

in the bulk concentration and electrode potential (more details about this dependence are given below, in the discussion of the results for higher concentrations). Finally, for both of the premicellar solutions shown here, a deformed peak is recorded at negative potentials. This is likely to result from the merge of a peak corresponding to the phase change of surface aggregates to adsorbed monomers (as the potential becomes more negative) with the peak of monomer desorption from the electrode surface (as the potential becomes even more negative). Note that under equilibrium conditions and at concentrations below the cmc (where there are no aggregates in the bulk solution), any surface aggregates will have to be transformed into adsorbed monomers before they are desorbed as monomers from the solution. The above findings could be explained if we accepted that, even at concentrations below the cmc, the adsorbed surfactant exists in the form of surface aggregates/micelles. At the molecular level, one could speculate the Tween-80 molecules as having a tilted orientation with most of their hydrophobic monoesteric segment (see Figure 1b) in contact with the mercury surface and their hydrophilic segment facing the aqueous solution. This orientation would allow for surface association into two-dimensional patches via hydrophobic tail-to-tail interactions between a large (but finite) number of adsorbed monomer units. Unless other phenomena such as reorientation, interaction of the first layer with outer layers, and formation of three-dimensional aggregates are present (from -0.6 to -1.3 V for higher concentrations, see the detailed discussion below), the higher the bulk and surface concentrations are, the larger the two-dimensional surface aggregates will be, and the less the coadsorbed water will be present.[19] The last two facts result in lower capacitance values with increasing surfactant concentration, as indeed is the case in the 0 to -0.6 V and -1.2 to -1.6 V potential ranges.

The C vs E picture changes significantly for the postmicellar concentrations studied, i.e., for 5×10^{-5} (shown in Figure 3), 10^{-4}, and 5×10^{-4} M (last two not shown). In fact, the curves for all of these concentrations were identical to within the experimental error. The peak at negative polarizations is higher than those of the premicellar solutions, less broad and sharper, as expected for larger surface aggregates.[19] There are two distinct regions of low capacitance, one between -0.1 and -0.5 V ("anodic plateau", minimum value of ca. 5 μF/cm^2) and another between -1.2 and -1.6 V ("cathodic plateau", minimum value of ca. 8 μF/cm^2). The curved shape of these plateaus is quite different not only from the completely flat pit of condensed layer,[35] but also from the extended plateaus we previously observed for closely packed patches of adsorbed aggregates.[20−25] In either of these cases, the bulky polymeric surfactant Tween-80 would have given rise to extremely low capacitance values. Instead, a looser structure, consisting of distinct surface aggregates and residual water, is more likely to exist, based on the present results. One could envisage the presence of hemispherical aggregates ("hemimicelles"[48]) with a circular hydrophobic monoesteric base in contact with mercury and a polar polyoxyethylene hemisphere facing the solution in the anodic plateau region (Figure 1b). The opposite arrangement (polar part of the aggregates of the first layer on the electrode surface and hydrophobic part toward the solution) is expected for the cathodic plateau region, whereby the first layer is further stabilized by its interaction with the hydrophobic segment of a second adsorbed layer that starts to develop at high concentrations (Figure 1e). Between these two plateaus lies a deformed and broad hump, corresponding to the reorientation of the adsorbed monomer units with the positive end of the dipole of the hydrophilic part toward the negatively charged electrode (Figure 1c,d). This starts to develop even below the cmc but becomes significant only at high concentrations. The fact that this reorientation/formation of two different adsorbate states depends not only on electrode potential but also on surfactant concentration indicates a strong influence of adsorbate−adsorbate interactions on the reorientation process. This could be the effect of at least one additional (not necessarily saturated) adsorption layer on the underlying film integrity (Figure 1c). Hence, no reorientation hump is observed for the lowest concentration studied (5×10^{-6} M). The broadness and deformation of this hump, which is attributed to a phase change (reorientation), could be explained if the above-mentioned process were realized via a number of steps, each with its own transition potential. At the molecular level, a possible interpretation of the transformation of the anodic plateau into the cathodic one at high concentrations within the multilayer adsorption hypothesis is that, as the potential becomes more negative from the potential of zero charge and maximum adsorption (ca. -0.5 V),[49] the two-dimensional hemimicelles of the first adsorption layer are transformed into three-dimensional, weakly adsorbed surface aggregates (Figure 1d). This results from the partial reorientation of their monomer units through simultaneous interaction with an outer adsorption layer (Figure 1c). These spherical, bulklike micelles are expected to form a less cohesive film, hence the increase in capacitance around the hump at intermediate polarization. As the electrode potential becomes more negative, the electrode−adsorbate dipole interactions become stronger than the adsorbate−adsorbate ones (which hold the spherical micelles together), and the polar group of the adsorbate is firmly attached to the negatively charged electrode surface. Thus, in this case, the Tween-80 aggregates of the first layer have their polar part toward the electrode, while the adsorbate monomers of the second layer still have them facing the solution (Figure 1e). Such a loose "bilayer" structure (containing water around the polar heads) has already been proposed as a part of Tween-80 liquid crystals.[11] Finally, the shape of the single cathodic peak at ca. -1.8 V could be explained if the shape were associated with the transition of the surface micellar film to adsorbed monomers and their desorption into the postmicellar solution as spontaneously formed bulk micelles. As described in refs 17−19, the transformation of an adsorbed layer that consists of associated adsorbate molecules (surface aggregates or micelles) rather than a continuous single-entity layer is expected to give rise to bell-shaped peaks of finite height.

Kinetics of Film Formation. In the case of phase formation on a surface, on the basis of the Avrami theorem[28] for two-dimensional phase formation, the true surface coverage θ of the new phase should be replaced by a fictional "extended" surface coverage θ_{ext}, which the new phase would have occupied had it continued in uninhibited growth via neighboring growth centers or the finite surface area available. The relation between the true and extended surface coverage should be written as

$$\theta = 1 - e^{-\theta_{ext}} \qquad (3)$$

If we accept that changes of the condensed-film surface

(48) Somasundaran, P.; Fuersternau D. W. *J. Phys. Chem.* **1966**, *70*, 70.

(49) Milberg, G.; Kratohvil, J. P.; Zeeman, P. *J. Colloid Interface Sci.* **1988**, *126*, 63.

coverage at the mercury/solution interface with time affect (decrease) the differential capacitance C in a linear manner, then we can write[26]

$$\theta = \frac{C_{in} - C}{C_{in} - C_{fin}} \quad (4)$$

where C_{in} is the initial capacitance value collected immediately (or, more realistically, shortly) after the application of the potential step and, therefore, corresponding to an adsorbate-state phase other than that of the condensed film (in our experiments, the capacitance was collected after 0.2 s, the first sampling time) and C_{fin} is the final, steady-state value corresponding to the new, condensed phase formed. C_{fin} is the saturation capacity (full coverage of the surface by the condensed phase) and not merely the equilibrium capacitance. Only if there are different condensed adsorbate states at different electrode potentials does its value changes with potential.

From eqs 3 and 4, it follows that

$$\theta_{ext} = \ln \frac{C_{in} - C_{fin}}{C - C_{fin}} \quad (5)$$

If the mechanism of the new phase formation can be described in simple nucleation and two-dimensional growth terms then, as it was shown in ref 29 and applied to adsorption processes by Retter,[31] the extended surface coverage is given by

$$\theta_{ext} = bt^m \quad (6)$$

where the constant b depends on the nucleation and growth rates and m indicates the number of steps required for the formation of a stable nucleus of the new phase. Then, according to the Avrami formalism (as follows from eq 6), a plot of $\ln \theta_{ext}$ vs $\ln t$ (Avrami plot) should be linear, and its slope should provide more details about the transition mechanism; an Avrami slope of $m = 2$ suggests a phase formation via instantaneous nucleation and two-dimensional growth, whereas a slope of $m = 3$ suggests progressive nucleation and two-dimensional growth[29-33] under constant growth rates.

To account for special cases of condensed film formation that lead to C vs t transients showing an equilibrium condensed-phase surface coverage θ_{eq} and capacitance C_{eq} which are dependent on the electrode potential (the case of 2-thiohydantoin from acetonitrile solutions), a "reversible phase transition" model has been proposed.[37] According to this model (referred to as model A hereafter), the equilibrium state is due to the presence of condensed adsorbate islands that only partially cover the electrode surface, and there is a dynamic equilibrium between adsorption at the periphery of the islands and desorption at their center. Momentary degree of condensed film coverage θ and its equilibrium value θ_{eq} are defined as

$$\theta = \frac{C_0 - C}{C_0 - C_1} \quad (7)$$

$$\theta_{eq} = \frac{C_0 - C_{eq}}{C_0 - C_1} \quad (8)$$

where C and C_{eq} are the momentary and equilibrium capacitances, respectively, C_0 is the capacitance corresponding to condensed-phase coverage equal to 0, and C_1 is the capacitance corresponding to a closely packed condensed phase at full coverage.

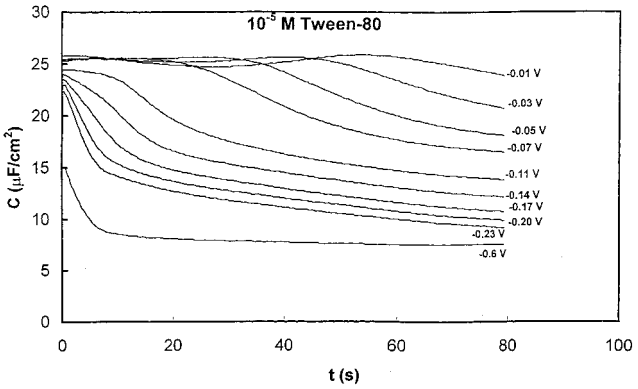

Figure 6. Capacitance transients following a potential step from −1.9 V vs SCE to potentials in the −0.01 to −0.6 V range, as indicated in the figure, for 1×10^{-5} M Tween-80 in 0.1 M Na_2SO_4 solution, as indicated in the figure.

On the basis of the dynamic adsorption/desorption equilibrium described above, it can be shown that

$$\ln (1 - (\theta_{eq}/\theta)^{1/2}) = -k(t - t_i) \quad (9)$$

where k is the desorption constant and t_i is the induction period for the formation of stable condensed-phase nuclei.

Substituting eqs 7 and 8 into eq 9 gives

$$C = C_0 - (C_0 - C_{eq})[1 - \exp(-k(t - t_i))]^2 \quad (10)$$

The theoretical description of rising C vs t transients has also been attempted recently by Retter et al.[38] for the case of octanoic acid adsorption on Hg.

According to one model (referred to as model B hereafter), the rise of the capacitance is due to the adsorption-controlled replacement of one condensed saturated adsorption state a with another condensed saturated adsorption state b having a higher capacitance value. This could be achieved, for example, by a reorientation of the adsorbate as the electrode potential changes. If C_a and C_b are the saturation capacitance values of the two states a and b and k is a constant containing the adsorption and desorption rates,[38] then

$$C = C_a - (C_a - C_b)[1 - \exp(-kt)] \quad (11)$$

In an alternative model for the same phenomenon, the transformation was considered for a condensed saturated state to a noncondensed one by desorption of adsorbate molecules from the condensed film and their adsorption/deposition on top of condensed islands, thus forming surface clusters/micelles. Assuming that the formation of the latter obeys the Avrami law, the following equations were derived corresponding to instantaneous and progressive nucleation, respectively (referred to as models C1 and C2 hereafter).

$$C = C_a - (C_a - C_b)[1 - \exp(-bt^{3/2})] \quad (12)$$

$$C = C_a - (C_a - C_b)[1 - \exp(-bt^{5/2})] \quad (13)$$

***C* vs *t* Curves.** Experiments where the capacitance variation of the mercury/solution interface with time was recorded after a potential step from −1.9 V vs SCE (where no Tween-80 adsorption occurs) to potentials in the −1.8 to 0.0 V range are presented for one premicellar (10^{-5} M) and one postmicellar (5×10^{-5} M) concentration.

Figure 6 shows a series of chronoamperometric ("chronocapacitometric") curves recorded for a 10^{-5} M Tween-

80 solution after the potential steps in the region of the anodic plateau in Figure 3 (a plateau which is ill-defined for this low concentration). It can be seen that exceptionally long induction periods of relatively constant capacitance values are observed and that their duration decreases toward the center of the capacitance well, in accordance with the nucleation and growth theories of phase transitions,[27,35] which state that before the growth of a new phase proceeds to a measurable extent, an induction period must pass, during which stable nuclei are formed and no macroscopic change occurs (in this case, no capacitance change). However, these results differ from the typical picture of phase transitions on mercury in that both the initial and final states of the adsorbate (reflected in the corresponding capacitance values) vary with the electrode potential. This is expressed as a curvature in the C vs E curves and can be explained if the nature of the new phase (e.g., the size of surface micelles) depends on adsorbate surface coverage, which itself changes with electrode potential, as discussed previously. The surface aggregates can be two-dimensional hemimicelles with the hydrophilic segment of their monomers toward the solution (see previous section and Figure 1b). Figure 7 attempts to apply Avrami plot analysis for two-dimensional phase transitions to the results. It is clear, however, that such a plot does not have a single slope throughout the (long) period. Instead, two slopes m are observed, as presented in the insets: a short-duration slope ($m = 1.3$ for $t < 10$ s) and a long-duration slope ($m = 0.58$ for $10 < t < 60$ s). Avrami plots with a changing or noninteger slope have been reported on a number of cases,[51−53] and it was suggested that they could be attributed to either coverage-dependent nucleation and growth parameters[52] or nonuniform three-dimensional growth.[53] Nonuniform growth might be due to the formation of a film of Tween-80 surface micelles resulting from the association of adsorbed monomers on a partially covered interface (containing also adsorbed water) with outer adsorption layers (likely to be present, especially at higher concentrations).

At this point, we should add that plots of C vs $1/t$ and C vs $\log t$ did not show any linearity for either concentration, ruling out the possibility of simple Elovich[53,54] or Langmuir[55] adsorption kinetics.

Figure 8 shows the capacitance variation with time for the 5×10^{-5} M Tween-80 solution following potential steps from −1.9 V into the well-defined anodic plateau (Figure 3). It can be seen that, as for the premicellar concentration, S-shaped curves are observed, but the induction period is much shorter (less than ca. 1 s) now and less dependent on electrode potential, indicating that the nucleation rate is a function of surfactant surface and (hence) bulk concentration, too. The Avrami plots in the inset exhibit a changing slope again ($m = 1$ for $t < 10$ s and $m = 0.63$ for $t > 10$ s), with values not far from those of the premicellar solution. Thus, in this case too, two-dimensional surface micelles are formed with sizes different (larger) than those of surface micells at the lower concentration, since the surface concentration is expected to be higher now. It should be noted that the application of simple Avrami analysis assumes that the steady-state equilibrium capacity of all corresponding transients corresponds to saturation. Since it is clear from Figures

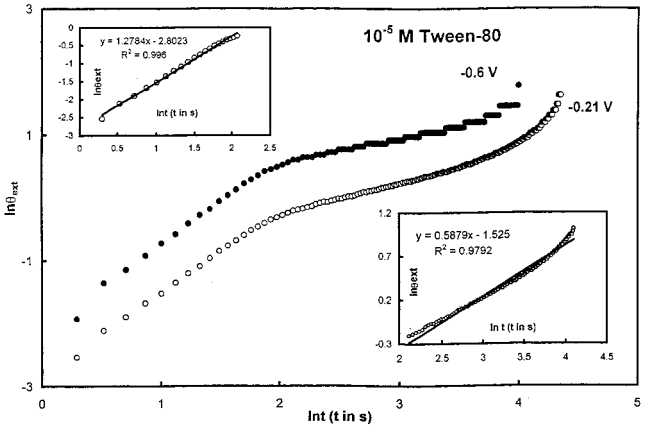

Figure 7. Avrami plots corresponding to potential steps from −1.9 V vs SCE to −0.21 and −0.6 V, as shown in the figure, for 1×10^{-5} M Tween-80 in 0.1 M Na_2SO_4 solution: top left-hand-side inset, short-duration part of the curve for −0.6 V; bottom right-hand-side inset, long-duration part of the curve.

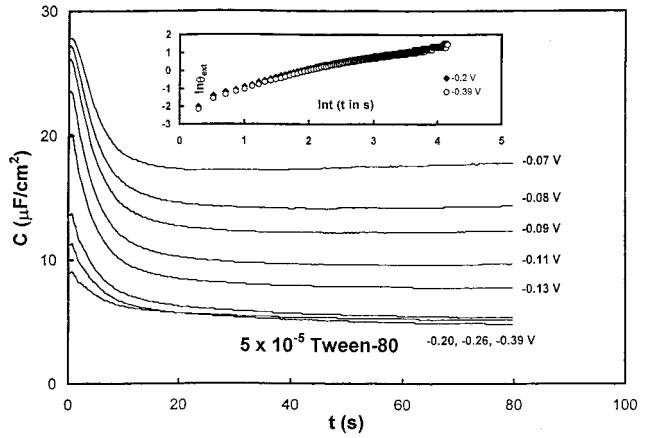

Figure 8. Capacitance transients following a potential step from −1.9 V vs SCE to potentials in the −0.07 to −0.39 V range, as indicated in the figure, for 5×10^{-5} M Tween-80 in 0.1 M Na_2SO_4. Inset: Avrami plot of the results at −0.2 and −0.39 V.

7 and 8 that this equilibrium capacity is different for different potential values, this assumption can be true only if the equilibrium adsorbate surface states are different (e.g., different orientation or aggregation) at different electrode potentials.

The application of model A of eq 10 (corresponding to a dynamic equilibrium of condensed adsorbate islands, whereby the rate of adsorption at the periphery of the islands is equal to the rate of desorption from their center) to the transients of Figures 7 and 8 did not result in a good fit with the data (mean specific deviations were between 2 and 5% when the iteration technique of the Solver Microsoft Excell tool was used).

In Figure 9, potential steps into the region of the second ill-defined plateau (to −0.9 and −1.1 V) for the 10^{-5} M concentration are depicted, together with a step to the first plateau region (−0.7 V) for comparison. A common feature of the first two transients is the initial fall of the capacitance to a minimum and its subsequent rise (after 10−25 s depending on the potential) to a steady-state value. We have observed this type of transient on a number of occasions during the study of the adsorption of micelle-forming surfactants on Hg,[20−25] and we attribute it to reorientation and/or interaction of the first adsorbed layer with outer layers. In the case of premicellar concentrations where multilayer adsorption is less likely, the proposed

(50) Damaskin, B. B. *Dokl. Akad. Nauk. SSSR* **1962**, *144*, 1073.
(51) Sridharan, R.; De Levie, R. *J. Electroanal. Chem.* **1986**, *201*, 133; **1987**, *230*, 241.
(52) Wandlowski; De Levie, R. *J. Electroanal. Chem.* **1993**, *349*, 15.
(53) Pospisil, L.; Svestka, M. *J. Electroanal. Chem.* **1994**, *366*, 295.
(54) Elovich, S. Y.; Zhabrova, G. M. *Zh. Fiz. Khim.* **1939**, *13*, 1761.
(55) Reddy, A. K. N. In *Electrosorption*; Gileadi, E., Ed.; Plenum Press: New York, 1967; p 53.

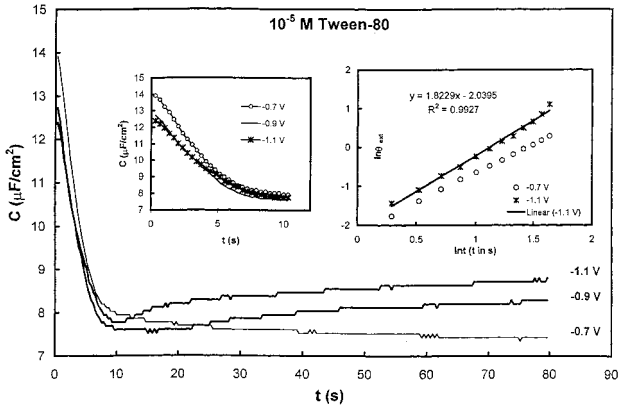

Figure 9. Capacitance transients following a potential step from −1.9 V vs SCE to potentials in the −0.70 to −1.1 V range, as indicated in the figure, for 1×10^{-5} M Tween-80 in 0.1 M Na_2SO_4 solution: left-hand-side inset, short-duration segment of the transient; right-hand-side inset, Avrami plot of the results.

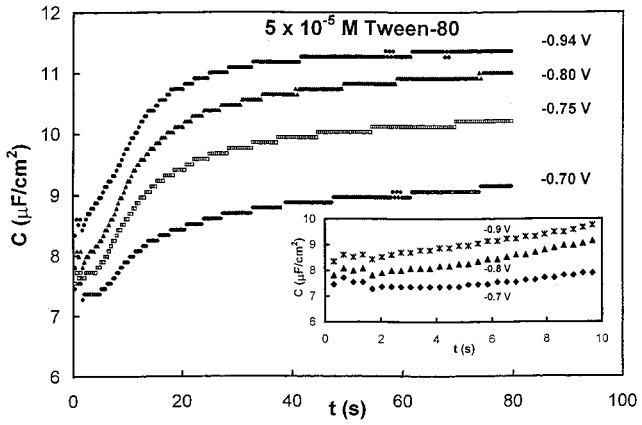

Figure 10. Capacitance transients following a potential step from −1.9 V vs SCE to potentials in the −0.70 to −0.94 V range, as indicated in the figure, for 5×10^{-5} M Tween-80 in 0.1 M Na_2SO_4 solution. Inset: Short-duration segment of the transient.

reorientation from a structure where the adsorbate monomer units have their polar heads toward the solution to a structure with their hydrophobic segments facing the solution could result from the electrostatic interaction of the negatively charged (beyond the ca. −0.5 V potential of zero charge) electrode with the oxyethylene-containing dipole of the hydrophilic part of Tween-80. As it is seen from the left-hand-side inset, the falling part of the transient does show some S-shape characteristics with a weakly defined induction period. The Avrami plot of the right-hand-side inset is linear over an appreciable time range, but again, a noninteger slope of 1.82 is observed.

Figure 10 presents results for potential steps into the capacitance "hump" region for the postmicellar 5×10^{-5} M solution. The S-shaped curves correspond now to capacitance values that increase with time. The inset shows clearer the short-duration (t <10 s) characteristics of the transients that have a local minimum around 2 s before the transients start to rise again. The initial increase in the capacitance up to ca. 1 s could be due to the fact that adsorbate monomers reorient partially, shortly after the application of the pulse, to a position where the polar group starts to approach the electrode surface (under the influence of the weakly charged electrode on its dipole), while the hydrophobic monomer gradually starts to tilt too until it faces the solution. The subsequent local minimum could be attributed to the two-

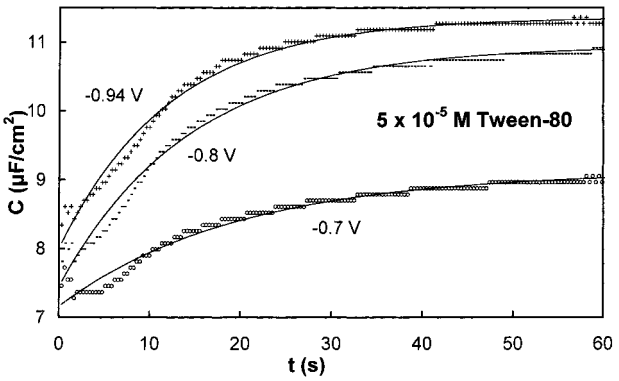

Figure 11. Fit of selected capacitance transients of Figure 10 (points) to model B (solid lines). The values of the adjustable parameters are given in Table 2.

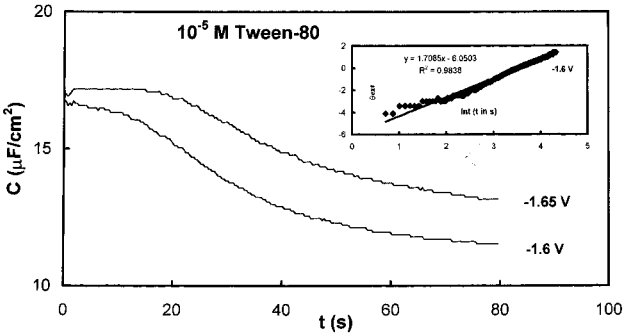

Figure 12. Capacitance transients following a potential step from −1.9 V vs SCE to −1.6 and −1.65 V, as indicated in the figure, for 10^{-5} M Tween-80 in 0.1 M Na_2SO_4 solution. *Inset:* Avrami plot for the −1.6 V transient.

Table 2. Parameters Used for the Best Fit of Eq 11, Model B, to the *C* vs *t* Transients in the Capacitance Hump Region for 5×10^{-5} M Tween-80 in 0.1 M Na_2SO_4 Solution[a]

E/(V vs SCE)	C_a/(μF/cm^2)	C_b/(μF/cm^2)	k (s^{-1})	Δ (%)
−0.7	7.16	9.12	0.051	0.5
−0.8	7.45	10.94	0.067	0.6
−0.94	8.00	11.36	0.082	0.5

[a] Δ denotes the mean percentage variation between experimental and estimated capacitance values.

dimensional association of these horizontal monomer units into flat surface micelles (Figure 1e). As time passes, the interaction of the hydrophobic part of monomers of an additional adsorbed layer with the hydrophobic core of these flat micelles further reorientates their monomers and forms near-spherical, three-dimensional micelles with hydrophobic cores and hydrophilic cells in contact with the electrode and the solution (Figure 1d). These autonomous entities are expected to form a noncohesive film of an open structure, hence the increase in capacitance.

Fitting the C vs E data to the curves of eqs 11, 12, and 13 (models B, C1, and C2, respectively) with the iteration technique used by the Solver tool of Microsoft Excel revealed a reasonable fit (mean variation was 0.4−0.5%) in model B, the one that assumed the replacement of one (saturation) adsorbate state to another by means of adsorbate unit reorientation.[38] The results are shown in Figure 11 and Table 2. The fact that the fit is not so good for short times (t <10 s) could be due to the time needed for the nucleation and growth to saturation of the initial adsorbate state.

Figure 12 shows capacitance transients after potential steps at the negative verges of the cathodic plateau for

Table 3. Slopes of Avrami Plots Corresponding to *C* vs *t* Transients after Potential Steps in Regions of Minimum Capacitance for 10^{-5} M Tween-80 Solutions[a]

E/(*V* vs SCE)	*m*
−0.6	1.28 ± 0.2
−1.1	1.82 ± 0.15
−1.6	1.71 ± 0.25

[a] Estimated deviations are given to with a 95% confidence interval.

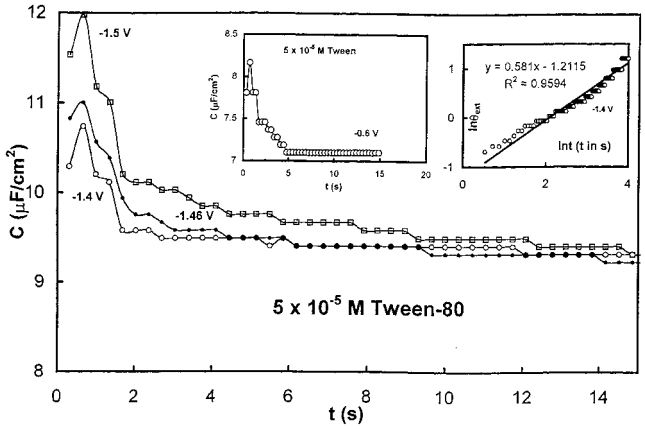

Figure 13. Capacitance transients following a potential step from −1.9 V vs SCE to potentials in the −1.4 to −1.5 V range, as indicated in the figure, for 5×10^{-5} M Tween-80 in 0.1 M Na_2SO_4 solution: left-hand-side inset, transient at −0.6 V; right-hand-side inset, Avrami plot of the −1.4 V transient.

the 10^{-5} M Tween-80 solution. The induction periods for the changes after potential steps at −1.65 and −1.6 V are longer than those required for similar changes (surface aggregation) at the positive verges of the anodic plateau (Figure 6), indicating that the nucleation rate of the surface micelles at negative polarization is lower than that of the surface micelles at positive polarization. Considering the structure of both types of micelles as discussed previously, we conclude that the intermolecular hydrophilic interactions are less favorable than the hydrophobic ones for Tween-80 adsorbed on Hg. The Avrami plot for −1.6 V in the inset of Figure 12 is also quite different (in the extent of linearity and slope) from that of Figure 7. Table 3 summarizes the Avrami plot results for 10^{-5} M Tween-80 at various potential regions.

Figure 13 shows capacitance transients after potential pulses in the region from the positive verges of the cathodic plateau up to its center (or, from another point of view, in the region negative to the "hump") for a 5×10^{-5} M solution. A complex but reproducible transient is observed, consisting of a distinct maximum and a subsequent S-shaped segment. In many similar cases (see above and refs 20−25), we have attributed any maxima or minima to the reorientation processes. We attribute the initial rise of the capacitance up to a maximum value after ca. 1 s to the reorientation of vertically adsorbed Tween-80 monomers, initially with their polar part toward the electrode in this potential region but then tilted to where their hydrophobic part can interact with the same part of the monomers of an outer adsorption layer (Figure 1c). In the center of the capacitance hump, these interactions result in three-dimensional micelles (Figure 1d), and the capacitance starts to rise again after the local maximum (Figure 10). In this case however, the stronger attraction of the polar part of the adsorbate by the electrode (stronger surface−adsorbate interactions) and the decrease of the adsorbate surface concentration as the potential is moved away from zero charge (weaker adsorbate−adsorbate

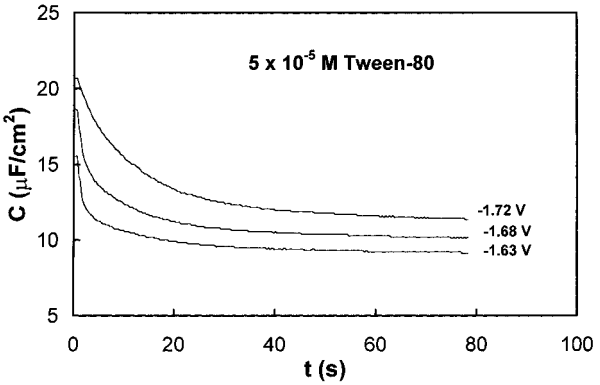

Figure 14. Capacitance transients following a potential step from −1.9 V vs SCE to potentials in the −1.63 to −1.72 V range, as indicated in the figure, for 5×10^{-5} M Tween-80 in 0.1 M Na_2SO_4 solution.

interactions) result in a destruction of these spherical micelles to fully orientated monomers that have their polar part toward the electrode. This results in a drop of the capacitance to a slowly changing value (at ca. 1.5 s) that corresponds to the induction period for the final formation of a more coherent layer of two-dimensional surface micelles, as in Figure 1e (final drop of *C* to its steady state value after ca. 2 s). An interesting finding is that, as shown in the left-hand-side inset, the same complex transient type was recorded at the positive verges of hump; this can be explained in a similar manner, with the only exception of the opposite orientations of the monomer units in the initial and final adsorbate states, due to the difference in the electrode charge. Finally, the right-hand-side inset presents an Avrami plot analysis of the second, S-shaped part of the transients.

In Figure 14, the results of potential step experiments in the negative potential verges of the cathodic plateau (and up to the cathodic peak) for the 5×10^{-5} M solution are shown. The shapes of the transients at −1.72, −1.68, and −1.63 V are very similar to those of the transients corresponding to the positive potential verges of the anodic plateau (Figure 8), and the Avrami plots (not shown for the cathodic plateau here) are very similar too. This suggests that the mechanism of formation and the type of surface aggregates are the same (two-dimensional hemimicelles) for both negative and positive polarizations and that only the monomer orientations differ.

Although the application of model A was not satisfactory for potential steps in the negative plateau region of the higher concentration, it gave a good fit (using the Solver tool of Microsoft Excel) in the case of the lower concentration. Figure 15 shows the results and indicates that the surface film at negative potentials of 10^{-5} M Tween solutions could consist of condensed islands (e.g., hemimicelles) that partially cover the electrode surface, while there is a dynamic equilibrium between adsorption at their periphery and desorption from their center.[37]

Conclusions

The study of the adsorption of Tween-80 on the polarized mercury electrode by means of differential capacity measurements, on the basis of both thermodynamic[17−19] and empirical considerations,[20−25] revealed that surface association of the adsorbate takes place for concentrations above and below the Tween-80 bulk cmc.

At concentrations far below the cmc, where no multilayer adsorption is expected, a single extended region of low capacitance is observed, attributed to small two-dimensional surface micelles. At concentrations above the bulk

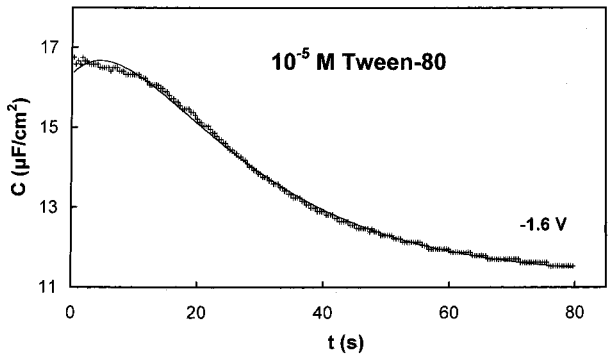

Figure 15. Fit of the capacitance transient for −1.6 of Figure 11 (points) to model A (solid line), using $C_0 = 16.67\ \mu F/cm^2$, $C_{eq} = 11.24\ \mu F/cm^2$, $k = 0.0495\ s^{-1}$, and $t_i = 4.5$ s in eq 10: parameters calculated by the Solver Microsoft Excell tool; mean deviation is 0.4%.

cmc, where multilayer adsorption could take place, a significant change of the *C* vs *E* curves is observed, the main features being two regions of low capacitance (attributed to two-dimensional surface micelles of different monomer unit orientations) and a broad hump between them (attributed to three-dimensional surface micelles). At concentrations between these two extremes, an intermediate picture is observed indicating that the type of surface aggregates formed is a function of interfacial surfactant concentration, which, in turn, depends on its bulk concentration up to the cmc point. Therefore, it should be noted that, although the *C* vs *E* picture changes significantly at concentrations around the bulk cmc for Tween-80 and all the ionic bulk micelle-forming surfactants that we studied,[20−25] signs of these changes are present even at lower concentrations, and therefore, correlation of these changes to the cmc values should be treated cautiously.

As first proposed by Damaskin[50] and recently argued by us on the basis of thermodynamic considerations of experimentally observed bell-shaped or deformed transition peaks,[17−25] surface aggregation can occur at concentrations well below the cmc, and therefore, the existence of surface micelles is independent of the presence of micelles in the bulk solution. Nevertheless, and since the surfactant solution activity remains constant beyond the cmc, the steady-state adsorbate surface concentration should also be independent of the total surfactant concentration beyond that point, and the corresponding *C* vs *E* curves should not change significantly above the cmc value. This is indeed the case for all the surfactant systems we studied, and the constancy of the *C* vs *E* curves with concentration is a safe criterion for the existence of micelles in the bulk solution.

It seems that, in general, significant changes in the *C* vs *E* curves of surfactant adsorption on mercury lead to significant multilayer adsorption, which, in turn, alters significantly the type of interfacial transitions taking place (which do not necessarily extend over a large number of layers). This multilayer adsorption concentration range may (as in the case of Tween-80) or may not coincide in general with the surfactant cmc.

No polylayer formation associated with very low capacitance values at extreme polarization is observed for the neutral surfactant Tween-80. Polylayer formation at extreme potentials (positive or negative) is a common feature of the adsorption of ionic surfactants (anionic or cationic, respectively) due to increased electrostatic interactions between the electrode and the adsorbate. This leads to very high interfacial surfactant concentrations and the formation of many closely packed saturated adsorbate layers.

The *C* vs *E* curves show very close and complex dependence on time, and thus, only the long-duration curves constructed by means of the potential step−capacitance sampling methodology can be considered as representative of the equilibrium under potentiostatic conditions. The capacitance transients recorded for regions corresponding to distinct surface states do not follow simple diffusion or adsorption kinetics, nor can they be analyzed according to the typical Avrami formalism (no linearity and noninteger slopes are observed), indicating mixed and/or complex phase formation mechanisms. Also, with the exception of the film at negative potentials for lower Tween-80 concentrations, film-formation kinetics cannot be described adequately from "reversible phase transition" model equations.[37]

Finally, the capacitance transients following potential steps in regions of the *C* vs *E* curves associated with three-dimensional surface micelles (such as peak shoulders and humps) seem to show the distinctive pattern[25] of a capacitance which is initially decreasing before increasing again (in a manner dependent on electrode potential) toward a steady-state value. The transients recorded for Tween-80 could be reasonably analyzed through a recent model proposed by Retter and co-workers which involves the replacement of a condensed adsorbate state with one that has adsorbate units of a different orientation and/or interactions.[38]

Acknowledgment. We are grateful to P. Lianos of the University of Patras for his help with fluorescence measurements.

LA991434E